ACS APPLIED MATERIALS & INTERFACES

www.acsami.org

Research Article

Biomimetic Upconversion Nanoplatform Synergizes Photodynamic Therapy and Enhanced Radiotherapy against Tumor Metastasis

Dandan Zhou, Yun Gao, Zhe Yang, Ning Wang, Jianxian Ge, Xiaoyi Cao, Dandan Kou, Yuan Gu, Cang Li, Mohammad Javad Afshari, Ruru Zhang, Can Chen, Ling Wen,* Shuwang Wu, Jianfeng Zeng,* and Mingyuan Gao

Cite This: *ACS Appl. Mater. Interfaces* 2023, 15, 26431−26441

Read Online

ACCESS | Metrics & More | Article Recommendations | Supporting Information

ABSTRACT: The easy recurrence and high metastasis of fatal tumors require the development of a combination therapy, which is able to overcome the drawbacks of monomodal strategies such as surgery, photodynamic therapy (PDT), and radiotherapy (RT). Taking the complementary advantages of PDT and RT, we present herein the integration of lanthanide-doped upconversion nanoparticles (UCNPs) with chlorin e6 (Ce6)-imbedded RBC membrane vesicles as a near-infrared-induced PDT agent for achieving synchronous depth PDT and RT with reduced radiation exposure. In such a nanoagent, gadolinium-doped UCNPs with strong X-ray attenuation ability act not only as a light transductor to activate the loaded photosensitizer Ce6 to allow PDT but also as a radiosensitizer to enhance RT. PDT with enhanced low-dose RT can achieve synergistic inhibition of tumor growth by producing reactive oxygen species to destroy local tumor cells and inducing strong T-cell-dependent immunogenic cell death to arrest systemic cancer metastasis. This combination of PDT and RT might be a potential appealing strategy for tumor eradication.

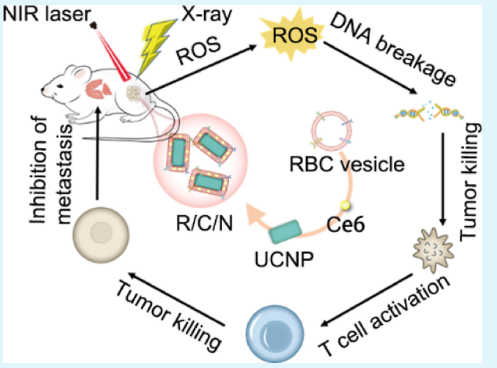

KEYWORDS: *upconversion nanoparticle, photodynamic therapy, radiotherapy, radiosensitization, tumor metastasis*

upconversion nanoparticle, photodynamic therapy, radiotherapy, radiosensitization, tumor metastasis

1. INTRODUCTION

Currently, cancer treatment centers around surgery, radiotherapy (RT), and chemotherapy. Among them, radiation therapy, including external beam radiation therapy and internal radioisotope therapy, has provided a potent local treatment method to prolong 3 and 5 year survival rates in patients.[1−3] However, suffering from the low tissue selectivity and strong penetration ability of ionizing radiation, the therapeutic efficiency is usually compromised by insufficient energy deposition in the tumor region and undesirable toxicity to normal tissues.[4−6] In this context, photodynamic therapy (PDT) with high specificity and controllability has been proposed to be combined with RT to improve treatment outcome.[4,7−10] This is mainly because PDT can exclusively transfer light energy to the tumor region, and the on−off status of PDT can be easily manipulated by tuning the light irradiation. In addition, the introduction of PDT can effectively reduce the radiation dose of regular RT.

PDT consists of three components: light source, photosensitizers, and oxygen.[11−13] It works by light excitation of photosensitizers, which in turn generates reactive oxygen species (ROS), such as singlet oxygen ($^1O_2$), in the presence of oxygen.[11−13] ROS can directly destroy tumor cells and the surrounding vasculature, resulting in obvious tumor ablation. Of note, PDT can activate systematic antitumor immune responses secondary to the primarily induced necrosis and/or apoptosis of tumor cells,[14] leading to enhanced immune cell infiltration and tumor antigen presentation,[10,14−16] which promotes the priming of tumor-specific T lymphocytes that are able to recognize and destroy tumor cells at primary and distant sites.[17,18] Among the selectable photosensitizers, Ce6 has been extensively reported as a highly efficient organic photosensitizer.[11] However, the absorbance of Ce6 always falls in the visible light region, where the light tends to be depleted through its penetration in a corporeal system and thus is suboptimal to reach targets, especially for deep-seated targets.[4]

For the purpose of breaking light-associated restrictions, upconversion nanoparticles (UCNPs) have emerged to offer a promising avenue to achieve effective PDT with reduced side effects.[19−22] Figuratively speaking, UCNPs act as internal energy transductors to convert low-energy photons to high-energy

Received: March 13, 2023
Accepted: May 11, 2023
Published: May 23, 2023

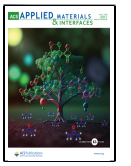

Scheme 1. Illustration of the Synthesis of R/C/N and the Synergetic Antitumor Effect of PDT Combined with RT

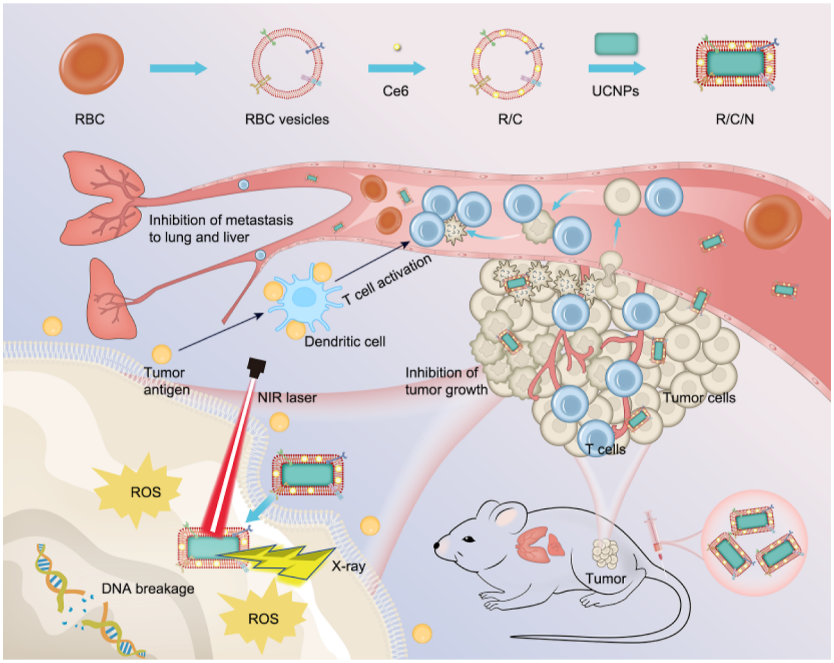

photons via the so-called anti-Stokes process, which can be performed by low-power and incoherent excitation sources.[23,24] As near-infrared (NIR) light (700−1300 nm) with a penetrating depth of several centimeters is accepted as the optimal exciting light,[25,26] NIR-controlled photodynamic therapies using UCNPs for energy transfer have ranked out among diverse precision treatment methods due to their noninvasiveness and high specificity.[11,24,27−29] In NIR-controlled UCNP-based PDT implementation, NIR light is absorbed by UCNPs to emit visible light, followed by the absorption of visible light by photosensitizers and subsequent excitation for ROS production.[29] It has been reported that the emission spectra of $NaGdF_4$:Yb,Er UCNPs match well with the absorption spectra of the photosensitizer Ce6, leading to potent activation of Ce6 to produce ROS for exerting a tumor killing effect.[30] Moreover, benefiting from the high-Z element Gd, the Gd-doped UCNPs possess powerful high-energy ionization radiation absorption ability to increase the intracellular radiation energy deposition, which prompts the popular exploration of Gd-based nanomaterials as radiosensitizers in recent years.[31,32]

With the aim of improving the biocompatibility of UCNPs that are supposed to be present in tumors simultaneously with photosensitizers before being subjected to laser irradiation, we took advantage of red blood cell (RBC) membrane camouflaged technology, which not only endows UCNPs with immune escape capability but also provides an ideal carrier for abundant loading of hydrophobic organic photosensitizers.[33−37] Liu et al. previously uncovered that Ce6 could be decorated into the RBC membrane upon simple mixing without affecting the membrane integrity and stability in the dark.[38] In addition, there is great possibility for RBC membrane-coated nanoparticles to enter wide clinical use when it comes true that type-matched RBCs are used as membrane sources to maximize biocompatibility.[35] Overall, the combination of Ce6-embedded RBC membranes and UCNPs represents a rational design to achieve coordinated RT and PDT triggered by NIR lasers.

Herein, R/C/N are constructed by coating Gd-doped UCNPs ($NaGdF_4$:Yb,Er) with a Ce6-loaded RBC membrane (Scheme 1). In such a nanoagent, while NIR-controlled upconversion luminescence of UCNPs can activate Ce6 to allow PDT, UCNPs containing gadolinium increasing the intracellular deposition of radiation energy could act as a radiosensitizer to enhance RT. As expected, the as-prepared R/C/N nanoparticles exhibit excellent stability and biocompatibility in physiological medium, making them appropriate for further applications. Upon NIR laser excitation, the R/C/N nanoparticles are able to produce abundant ROS for PDT. Thereby, PDT can enhance RT-associated DNA damage in tumor cells and promote tumor cell apoptosis. The combination of PDT and RT can induce tumor-specific antigen release and then effectively induce immunogenic cell death (ICD). Further results of animal experiments demonstrate that R/C/N-mediated PDT not only enhances the effect of RT to improve treatment outcome without obvious biotoxicity but also promotes T-cell-dependent antitumor immunity to suppress tumor growth and metastasis. Therefore, our work presents the great promise of R/C/N as a tumor therapeutic nanoplatform for cancer treatment.

2. RESULTS AND DISCUSSION

2.1. Synthesis and Characterization of R/C/N. First, we synthesized $NaGdF_4$:Yb,Er upconversion nanorods, as nanorods penetrate tumors more rapidly than nanospheres, possibly due to improved transport through pores.[39] Jain et al. strongly suggest that nanorods will be more effective drug carriers than nanospheres for antitumor therapy,[39] considering that even small improvements in transport rates can bring significant enhancements to therapeutic effectiveness.[40] Furthermore, red blood cell membranes were prepared by using the method reported by Gao et al.[33] and used to load hydrophobic photosensitizer Ce6 via simple mixing, resulting in the RBC/Ce6 complex (R/C) as the vehicle of UCNPs. Upconversion nanocrystals were synthesized by a high-temperature approach, and the resulting UCNPs were functionalized with PEG molecules to endow them with excellent hydrophilicity for

https://doi.org/10.1021/acsami.3c03636
ACS Appl. Mater. Interfaces 2023, 15, 26431−26441

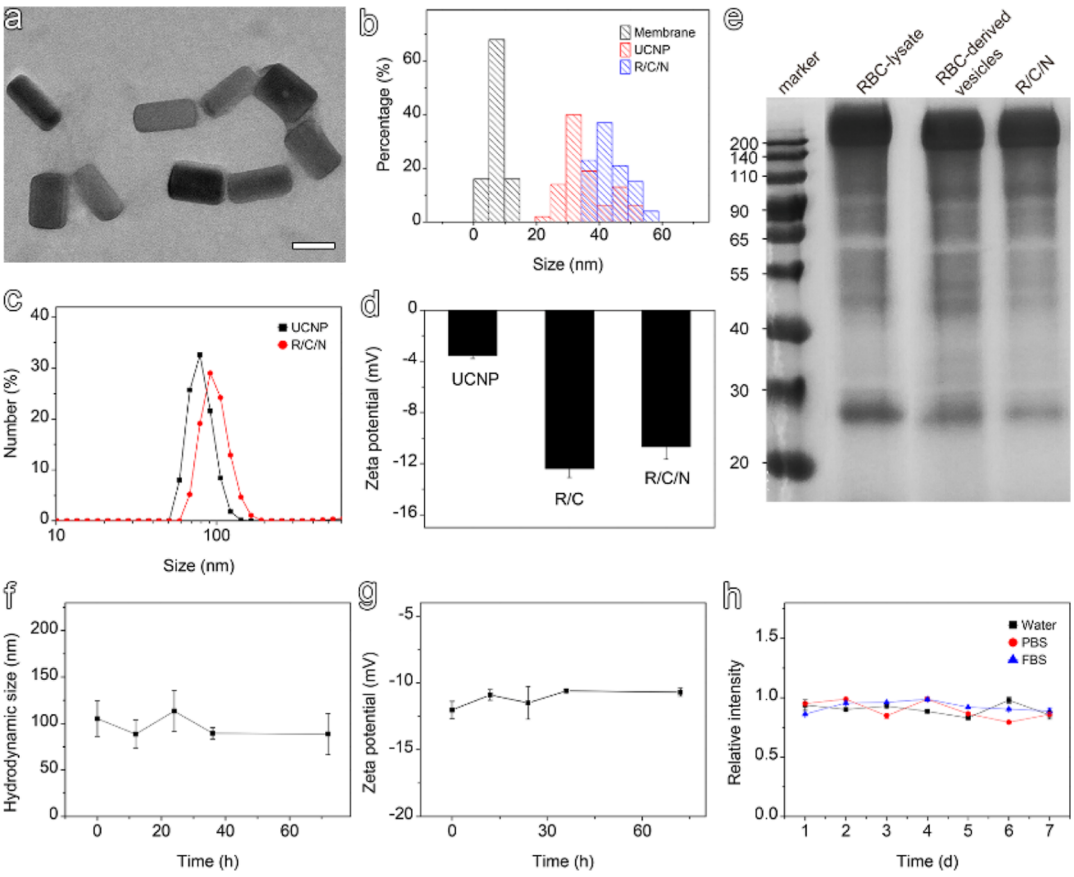

Figure 1. Synthesis and characterizations of R/C/N. (a) TEM image of R/C/N (scale bar = 50 nm). (b) Diameter/thickness histograms of membrane, UCNP, and R/C/N. (c) Hydrodynamic size distribution profiles of UCNPs and R/C/N. (d) Zeta potential of UCNPs, R/C, and R/C/N. (e) SDS−PAGE analysis results of RBC lysate, RBC-derived vesicles, and R/C/N. (f) Hydrodynamic size, (g) zeta potential, and (h) fluorescence stability of R/C/N.

further processing in an aqueous solvent. The final fusion of the as-prepared RBC/Ce6 complex and PEGylated UCNPs was achieved via an extrusion method to obtain the R/C/N nanoparticles.[41]

The morphologies of the UCNPs and R/C/N were characterized using transmission electron microscopy (TEM), as shown in Figure 1a,b, respectively. The prepared UCNPs were well-dispersed nanorods with an average diameter of 36.1 ± 7.3 nm and an aspect ratio (i.e., length to diameter) of ∼2. Upon coating, the obtained R/C/N exhibited a similar rod shape with a slightly larger diameter of 44.8 ± 5.3 nm and a clear layer of membrane structure. The thickness of the outermost shell was estimated to be 8.2 ± 2.1 nm from the TEM images, which was consistent with the thickness of the regular RBC membrane,[36] indicating successful encapsulation of UCNPs by the RBC bilayer membrane vesicles. Meanwhile, a thickness less than 10 nm is small enough to make sure that the imbedded photosensitizers are in proximity to the UCNPs for efficient energy transfer.

To further verify the successful coating of the RBC membrane, the hydrodynamic diameter and zeta potential of the UCNPs and R/C/N nanoparticles were measured. The dynamic light scattering (DLS) data revealed that UCNPs have an average size of 78.8 nm, while R/C/N nanoparticles exhibited an increased average size of 91.3 nm attributed to the existence of the RBC membrane (Figure 1c). In addition, zeta potentials were found to be −3.5 ± 0.2 mV, −12.4 ± 0.7 mV, and −10.7 ± 1.0 mV for UCNPs, R/C, and R/C/N, respectively (Figure 2d), reflecting a shift of the surface charges after coating with RBC membrane vesicles which possess a more negative surface charge than UCNPs. R/C/N and Ce6 emitted the same emission fluorescence at 660 nm under excitation with a 405 nm laser, which verified that Ce6 was successfully loaded on the erythrocyte membrane (Figure S2a). Considering that RBC membrane proteins play a vital role in immune evasion, the retention of membrane proteins on R/C/N nanoparticles was analyzed by sodium dodecyl sulfate−polyacrylamide gel electrophoresis (SDS−PAGE). Using the RBC lysate and RBC vesicles as parallel controls, the protein stripes of R/C/N presented very matched protein bands, as demonstrated in Figure 1e, which confirmed the preservation of membrane proteins during the purification and washing steps.

The fluorescence emission spectrum of R/C/N was recorded under excitation of a 980 nm laser. The results showed two remarkable emission peaks at 540 and 655 nm (Figure S2b). The UV−vis−NIR spectra of R/C/N nanoparticles peaked at 660 nm, which was very close to the emission peak under 980 nm light triggering (Figure S2b,c). The good overlap of the emission and absorption spectra of R/C/N nanoparticles implied that the upconversion photons from UCNPs encapsulated inside could be efficiently absorbed by the proximate Ce6 on the RBC membrane. Further monitoring for several days the hydrodynamic size, the zeta potential and fluorescence intensity demonstrated that the resulting UCNPs and R/C/N possessed excellent colloidal stability and fluorescent stability in an

https://doi.org/10.1021/acsami.3c03636
ACS Appl. Mater. Interfaces 2023, 15, 26431−26441

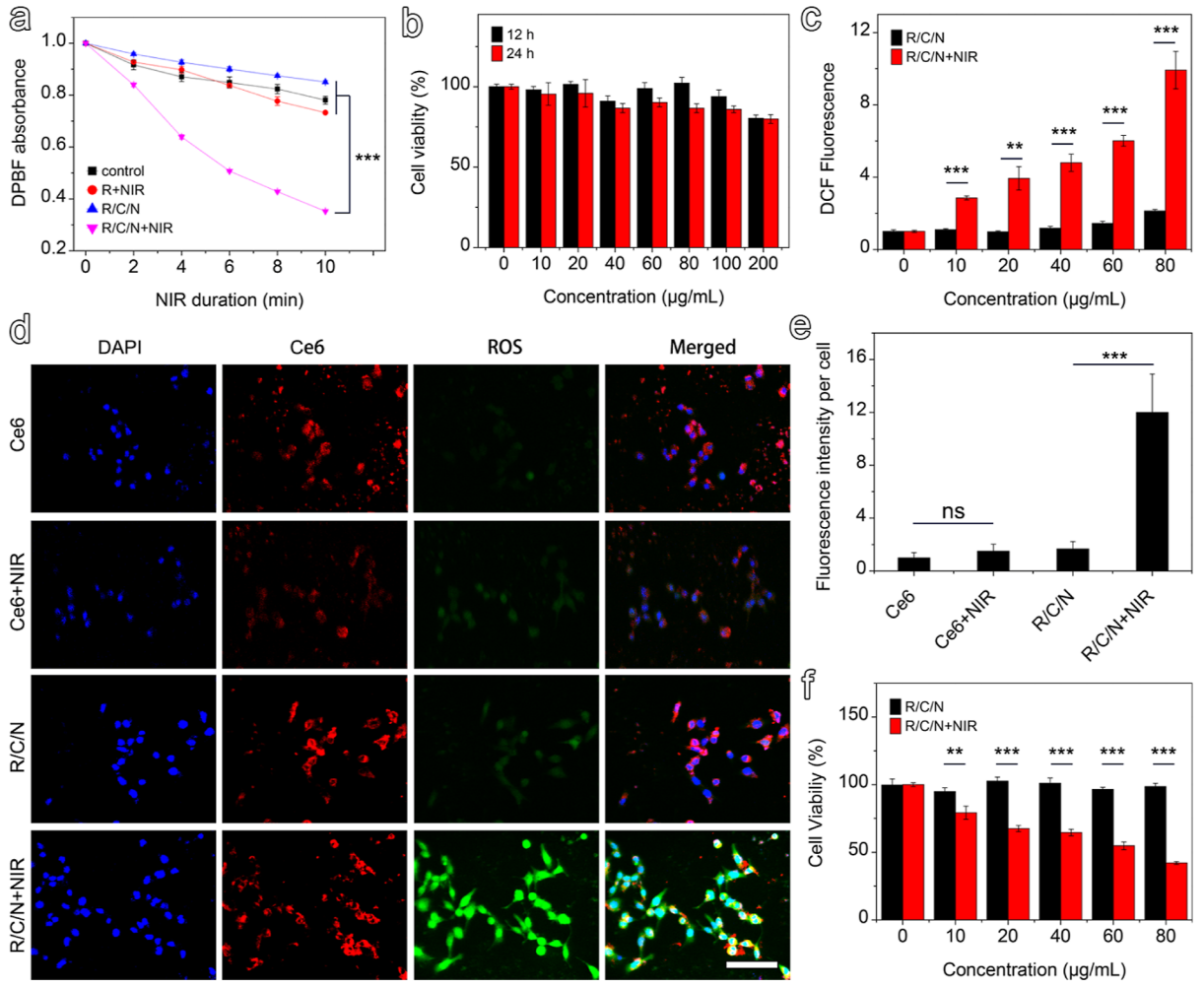

Figure 2. In vitro PDT with R/C/N. (a) Comparisons of ROS production among control and R/C/N group, RBC vesicle, and R/C/N groups following NIR laser irradiation at 980 nm (0.25 W cm^{-2}), as determined by the decay in DPBF absorbance, which was measured at its peak intensity of 410 nm. (b) Cell viability of 3T3 cells after various treatments indicated as evaluated by the standard MTT assay. (c) Concentration-dependent ROS generation by R/C/N under 980 nm laser irradiation. (d,e) Confocal fluorescence images (d) and ROS generation (e) of cells after NIR (980 nm, 10, 1 min interval, and 0.25 W cm^{-2}) laser light irradiation (scale bar = 100 μm). (f) Cell viability of 4T1 cells after various treatments evaluated by the standard MTT assay. Values are means ± SDs, $n = 3$, ns > 0.05, $^{**}P < 0.01$, and $^{***}P < 0.001$.

aqueous solution (Figures 1f,g and S3) and thus were eligible for in vivo applications.

2.2. In Vitro PDT and Cytotoxicity of R/C/N. As discussed above, R/C/N was successfully constructed to act as a potential nanotransductor of light for Ce6 activation on the basis of the close combination and overlapping emission and absorption spectra of Ce6 and UCNPs. Adequate ROS, particularly singlet oxygen $^1O_2$, is a prerequisite for an efficient PDT process. We used 1,3-diphenylisobenzofuran (DPBF) as a fluorescence probe to detect extracellular $^1O_2$ generation, which displayed absorbance loss at approximately 410 nm in the presence of ROS. As shown in Figures 2a and S4, the control, RBC vesicles + NIR laser, and R/C/N groups had no significant decrease in absorbance, indicating no significant ROS production. In contrast, there was a remarkable decrease in absorbance in the R/C/N + NIR laser group, evidencing the strong extracellular generation of ROS upon continuous NIR irradiation of R/C/N.

Prior to further examination of the potential of R/C/N nanoparticles in PDT, the biosafety issue, which is of very first importance for in vivo applications, needs to be addressed. To this end, we used normal somatic cells, 3T3 cells, as a cell model to evaluate the biocompatibility of R/C/N using typical MTT assays. The results revealed that the cell viability rates were over 80% after incubation for 12 h and 24 h at concentrations below 200 μg mL^{-1} (Figure 2b), demonstrating a negligible toxicity of R/C/N to normal cells. For living cells, 2′,7′-dichlorofluorescin diacetate (DCFH-DA) was used to detect intracellular ROS. Once diffused into cells, DCFH-DA is hydrolyzed into a nonfluorescent compound (DCFH), which can be oxidized by ROS to produce highly fluorescent 2′,7′dichlorofluorescein (DCF). In comparison to the cells treated with R/C/N without NIR laser irradiation, those that were incubated with R/C/N followed by exposure to NIR laser light (980 nm) showed markedly increased DCF fluorescence signals, confirming the production of intracellular ROS. In addition, the increased fluorescence signals positively corresponded to the incremental concentration of R/C/N (Figure 2c). The intracellular ROS level was further assessed by confocal laser scanning microscopy. Figure 2d shows that the green fluorescence induced by ROS was very weak in cells incubated with Ce6 and subjected to NIR (980 nm) laser irradiation. The reason is that Ce6 cannot directly utilize NIR light for ROS generation. However, it was found that R/C/N excited by the NIR laser caused a much stronger ROS-induced fluorescence intensity in cells by taking

https://doi.org/10.1021/acsami.3c03636
ACS Appl. Mater. Interfaces 2023, 15, 26431−26441

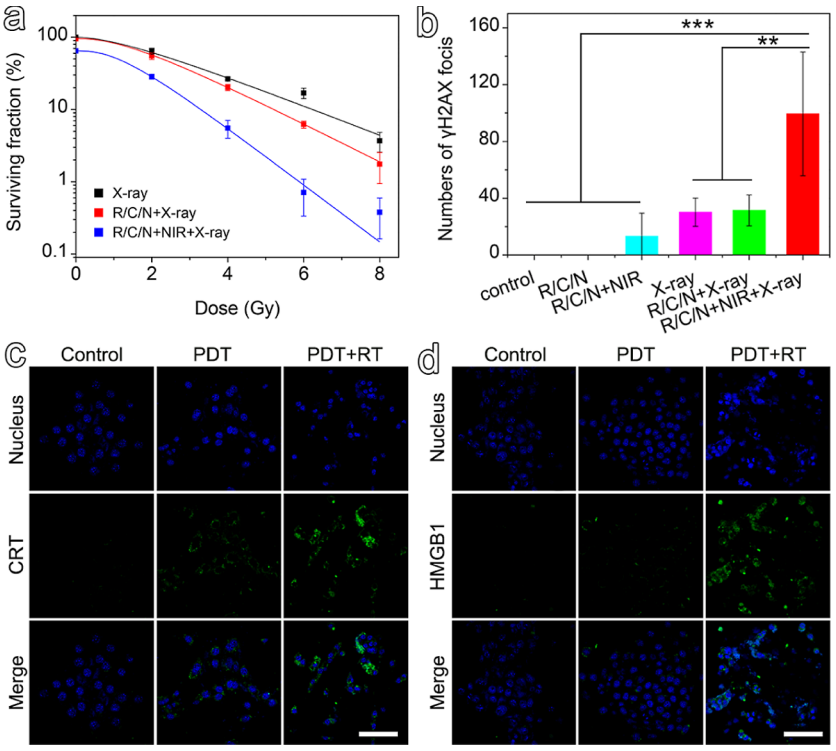

Figure 3. In vitro PDT combined with RT. (a) Cell viability for RT, R/C/N + RT, and PDT + RT on 4T1 cells. 4T1 cells were incubated with R/C/N (60 μg mL^{-1}), followed by varied doses of X-ray radiation (0, 2, 4, 6, and 8 Gy) and NIR irradiation (10, 1 min interval, and 0.25 W cm^{-2}). (b–d) 4T1 cells were incubated with R/C/N (60 μg mL^{-1}), followed by X-ray radiation (4 Gy) and NIR irradiation (10, 1 min interval, and 0.25 W cm^{-2}). (b) DNA damage of 4T1 cells with different treatments. Values are means ± SDs, $n = 3$, $^{**}P < 0.01$, $^{***}P < 0.001$. (c,d) In vitro CRT (c) and HMGB1 (d) exposure of 4T1 cells treated with PDT or PDT + RT (scale bar: 100 μm).

the cells solely treated with R/C/N as a parallel control, which was attributed to the UCNP acting as a light transductor to activate Ce6. The generation of ROS in cells was further quantified, as shown in Figure 2e. All these results confirmed that R/C/N is capable of considerably elevating ROS levels upon NIR triggering (Figure 2a,c–e). Following this confirmation, the R/C/N-based PDT effect was verified from the cellular viability via MTT assay on 4T1 tumor cells. Cell viability data revealed significantly reduced cell viabilities for 4T1 cells incubated with R/C/N after exposure to the NIR laser (10, 1 min interval, and 0.25 W cm^{-2}), in marked contrast to the nonirradiated cells, which showed no obvious cell death (Figure 2f). In addition, R/C/N resulted in concentration-dependent cell destruction upon NIR light exposure. Obviously, R/C/N had a remarkable photodynamic effect in tumor cells, making it a promising biomimetic nanoplatform for NIR laser-induced R/C/N-mediated PDT applications.

2.3. PDT Enhancement Effect on RT. Apart from the verification of the PDT effect, the potential of R/C/N for acting as effective radiosensitizers for RT was also investigated. Clone survival experiments were conducted to quantitatively evaluate the radiosensitization effect of R/C/N and PDT for 4T1 cells. According to the survival curves displayed in Figure 3a, under the same X-ray exposure, the colony formation derived from cells treated with the R/C/N + NIR laser markedly decreased in comparison to the cells that did not receive R/C/N treatment or NIR laser irradiation, suggesting a strong radiosensitivity enhancement of cells resulting from R/C/N + NIR laser treatment. This result was also reflected in the mean lethal dose (D_0) of X-rays, as the D_0 value of the R/C/N + NIR + X-ray group was determined to be 1.11 Gy, smaller than that of the R/C/N + X-ray group and X-ray group, which was 1.69 and 2.24 Gy, respectively, following the order of R/C/N + NIR + X-ray < R/C/N + X-ray < X-ray. Because the D_0 value is inversely related to radiosensitivity, it is reasonable to conclude that the radiosensitivity of 4T1 cells is improved not only by the UCNPs but also by the UCNP-induced PDT.

This argument was further proved by the immunofluorescence assay of γH2AX whose expression level reflects the DNA breakage caused by X-rays. As shown in Figures 3b and S5, although R/C/N itself did not cause DNA damage, as there was almost no fluorescence spot found in the R/C/N group, similar to the case of the control group, it could greatly promote DNA damage by X-ray triggering, as illustrated by the increased stained γH2AX in the R/C/N + X-ray group compared to that in the X-ray group. More importantly, compared with the R/C/N + NIR and R/C/N + X-ray groups, the R/C/N + NIR + X-ray group demonstrated the highest γH2AX foci, which indicated that the PDT process could also enhance RT-associated DNA damage in 4T1 cells and thereby lead to an improved killing effect on tumor cells. Furthermore, we used flow cytometry to examine the apoptosis effect of tumor cells. The results indicated that PDT could promote tumor cell apoptosis no matter if applied alone or combined with RT (Figure S6).

To study whether PDT alone or combined with RT can elicit ICD by triggering dying tumor cells to generate damage-associated molecular patterns, the biomarkers including the translocation of calreticulin (CRT) and the release of high-mobility group box 1 (HMGB1) of ICD were detected. The results in Figure 3c,d showed that PDT + RT treatment induced significantly increased expression of CRT and HMGB1 compared with the control and PDT groups. Therefore, R/C/

https://doi.org/10.1021/acsami.3c03636
ACS Appl. Mater. Interfaces 2023, 15, 26431−26441

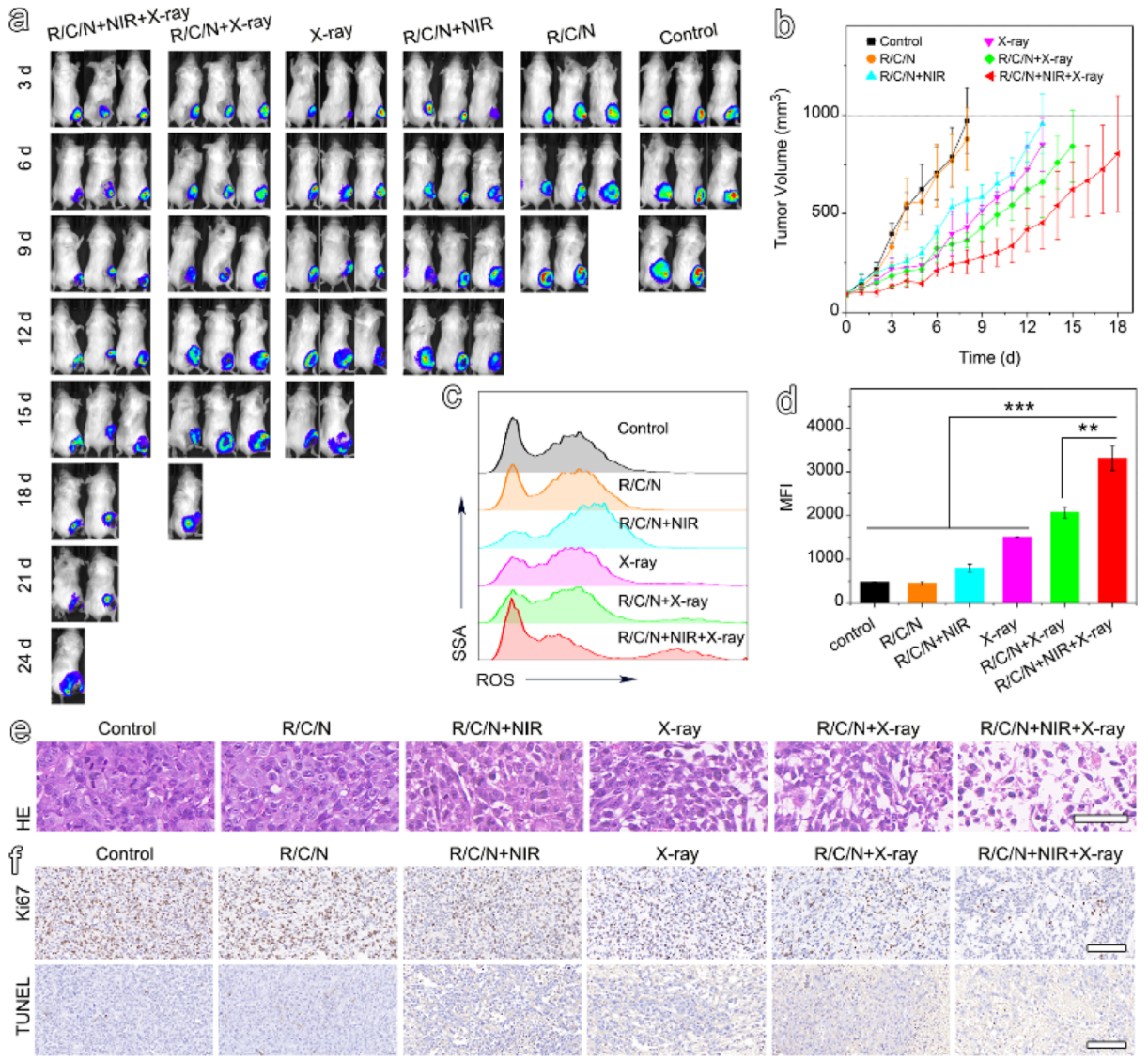

Figure 4. In vivo therapeutic effect assessment. Twelve hours after tail vein injection of PBS or R/C/N (0.1 mmol Gd per kg body weight), the tumors were irradiated by 6 Gy X-ray and/or NIR light (10, 1 min interval, 0.25 W cm^{-2}). (a) IVIS images of tumor-bearing mice with different treatments. (b) Corresponding growth curves of tumors in different groups of mice after treatments. (c) ROS generation in tumors treated with various treatments, as assessed by flow cytometry and (d) their corresponding MFI analysis. Values are means ± SDs, $n = 3$, $^{**}P < 0.01$, $^{***}P < 0.001$. (e) Pathological analysis of tumor sections (scale bar = 50 μm). (f) Representative images for Ki67 and TUNEL staining of tumor sections (scale bar = 100 μm).

N-mediated PDT combined with RT can effectively induce ICD.

2.4. Therapeutic Effect Assessment In Vivo. Encouraged by the synergistic damaging effect of PDT and RT on tumor cell viability, we performed in vivo antitumor experiments on 4T1 tumor-bearing mice. Before in vivo therapy, a histochemical staining method based on chlorophosphonazo III for analyzing rare-earth (RE^{3+}) in tissues was applied to monitor the R/C/N concentration in tumors and optimize the therapeutic time point.[42] According to the RE^{3+} concentration-dependent color changes of the standard solution and the staining images of tumor sections shown in Figure S7, 12 h postinjection was apparently the best time point for tumor therapy. In other words, at 12 h, the tumor region had the most desirable accumulation of R/C/N to allow the full exertion of the PDT process and radiosensitization effects.

Based on the above results, 4T1 tumor-bearing BALB/c mice were randomly divided into six groups and subjected to different treatments. The tumor volume of mice (Figure 4a,b) was monitored for weeks to evaluate the therapeutic efficacy of various treatments. On days 3−8, mice treated with only R/C/N did not exhibit an inhibitory effect on tumor growth compared with the control group, but with the help of the NIR laser, the tumor growth rate was obviously decreased due to the laser-induced PDT process. Compared with the X-ray group, the combination of R/C/N and X-ray was superior for slowing tumor growth, which further validated the radiosensitization effect of R/C/N. Among these various treatments, the R/C/N + NIR + X-ray group had the most potent inhibitory effect on tumors, with the smallest tumor volume all the time, proving the remarkable synergistic effects of PDT and RT on tumor regression. However, on days 9−15, except for the death of the control and R/C/N groups, the R/C/N + X-ray group or the R/C/N + NIR group also demonstrated limited inhibitory effects due to the easy recurrence of fatal tumors. Moreover, although the R/C/N + NIR + X-ray group did not eliminate the

https://doi.org/10.1021/acsami.3c03636
ACS Appl. Mater. Interfaces 2023, 15, 26431−26441

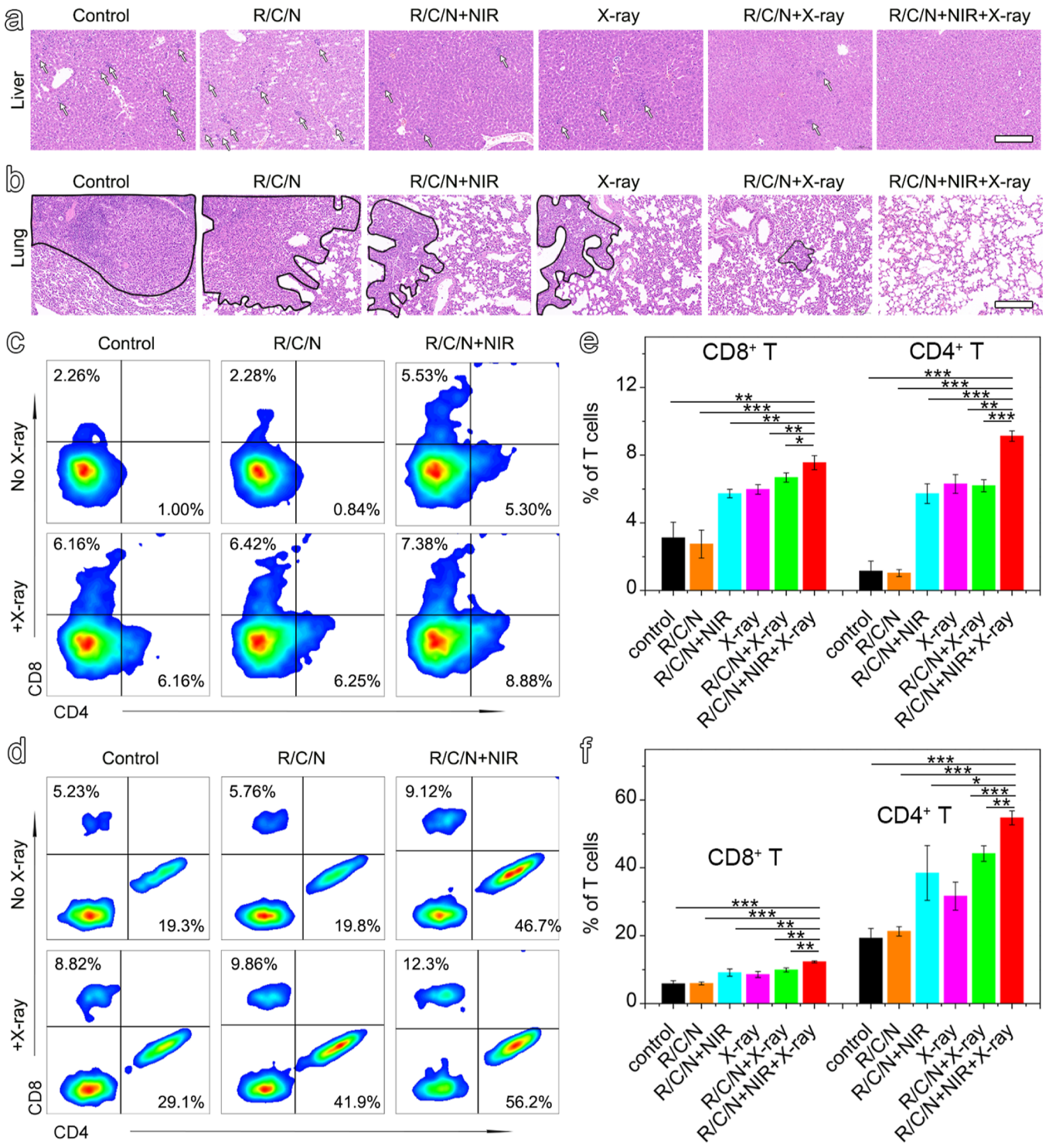

Figure 5. Inhibition of tumor metastasis. (a,b) H&E staining of liver metastasis (a) (indicated by white arrows) and lung metastasis (b) (indicated by the black line) in 4T1-tumor-bearing mice after various treatments (scale bar = 200 μm). (c,d) Representative flow cytometry plots of $CD8^+$ T cells and $CD4^+$ T cells in tumor-infiltrating $CD3^+$ lymphocytes in (c) 4T1 tumors and (d) PBMC from mice after various treatments for 3 days. (e,f) Quantification of $CD8^+$ T cells and $CD4^+$ T cells as a percentage of $CD3^+$ lymphocytes in (e) 4T1 tumors and (f) PBMC. Values are means ± SDs, n = 3. *P < 0.05, **P < 0.01, and ***P < 0.001.

malignant primary tumor, it greatly prolonged survival, leaving the largest treatment chance.

To better understand the above in vivo therapy results, the ROS level in the tumor tissues was determined based on the well-accepted knowledge that ROS-mediated DNA breakage predominates in cell death initiated by either PDT or RT.[8,43] Herein, flow cytometry was used to evaluate ROS production in tumor tissues. The tumors with different treatments were isolated and digested, and then the obtained tumor cell suspensions were incubated with DCFH-DA to detect ROS generation according to the fluorescence signal of DCF. Fluorescence-activated cell sorting files and their corresponding

https://doi.org/10.1021/acsami.3c03636
ACS Appl. Mater. Interfaces 2023, 15, 26431−26441

mean fluorescence intensity (MFI) (Figure 4c,d) revealed that the R/C/N + NIR + X-ray group had the strongest fluorescence signal among all the treatments, which indicated the most significant generation of ROS at the tumor site. From this perspective, the impact of the R/C/N nanosystem on achieving a combined treatment can be reasonably attributed to the synergistic augmentation of ROS generation.

The pathological tumor tissue sections obtained 8 d after treatment were used to further evaluate the treatment efficacy in vivo (Figure 4e). As clearly found in hematoxylin and eosin (H&E)-stained tumor sections, tumor tissues remained intact and undamaged in both the control group and R/C/N group, while an obvious damage occurred in the R/C/N + X-ray group. Notably, such damage became much more significant when the tissue was treated with R/C/N + PDT + X-ray, with the observation of prominent late-stage apoptosis. The highest level of tumor cell destruction shown in H&E staining slices further confirmed and again emphasized the combined effect of PDT and RT. In addition, we stained the tumor sections with Ki67 and TUNEL (Figure 4f). The statistical analysis results reflected that with the aid of R/C/N nanoparticles within PDT and RT, tumor cell proliferation was greatly inhibited, and tumor cell apoptosis was promoted, thereby leading to an enhanced antitumor effect (Figure S8). These results undoubtedly qualify R/C/N as a potential radiosensitization PDT agent.

Meanwhile, no significant weight loss or abnormal behavior was observed in the synergistic PDT and RT group (Figure S9). In addition, the pathological evaluation of H&E-stained sections from some important organs, such as the heart, kidney, and brain, showed no signs of inflammation, necrosis, or other damage, which further confirmed the excellent biosafety of the combination of R/C/N-mediated PDT and RT (Figure S10). To further study the toxicology of R/C/N, healthy female Balb/c mice intravenously injected with R/C/N were sacrificed at 7 days for complete blood counting and serum biochemistry tests. As shown in Figure S11, all the measured parameters of mice treated with R/C/N fell within normal ranges compared to the control. Considering the low retention of R/C/N in mouse major organs, including the heart, liver, spleen, lung, kidney, brain, stomach, small intestine, and large intestine, after 72 h, as shown in Figure S12, it might be reasonable to predict that R/C/N would not cause significant in vivo long-term toxicity.

2.5. Antitumor Metastasis Effect Evaluation. To examine the effect of antitumor metastasis, the liver and lung sections where tumor is prone to metastasize were collected for H&E staining (Figure 5a,b) by sacrificing mice under various treatments on the 8th day. The stained slices illustrated a similar trend of change of tumor metastasis in lung and liver. In addition, the statistical results of the number of pulmonary metastatic nodules are shown in Figure S13. Compared to the control group, the number of metastatic nodules was reduced to a great extent in mice treated with R/C/N + NIR or R/C/N + X-ray. Impressively, there is almost no tumor metastasis found on mice treated with R/C/N + PDT + RT.

Recent studies have highlighted the potentials of PDT alone or combined with RT to induce ICD of tumor (metastasis) by potentiating the systemic immunity.[18,44,45] Immunofluorescence images of representative tumors indicated that PDT alone and combined with RT treatment did increase the expression levels of CRT and HMGB1 compared to the controls (Figure S14). Furthermore, CD8 and CD4,[46,47] important immune makers of the cytotoxic T lymphocytes (CTLs) and helper T cells, respectively, were analyzed by flow cytometry (Figure 5c,d) to evaluate the change of immune cells in both primary tumors and peripheral blood mononuclear cells (PBMCs) from mice after various treatments. Flow cytometry analysis (Figure 5e,f) suggested the highest CTL infiltration in both primary tumors (7.6%) and PBMCs (12.3%) after treatment with R/C/N + NIR + X-ray, validating the essential role of T-cell-mediated immune response to efficiently inhibit tumor growth and metastasis. In detail, the recruitment of CTL after PDT combined with RT was 1.3- and 2.4-fold higher than RT and control groups in primary tumors, respectively. While in PBMCs, the recruitment of CTL after combined therapy was 1.4- and 2.1-fold higher than RT and control groups, respectively. In addition, R/C/N-mediated PDT combined with RT triggered the most significant infiltration of helper T cells in both primary tumors and PBMCs (Figure 5e,f), showing 1.4- and 1.7-fold higher than the RT group, respectively. Consistently, the populations of both CTLs and helper T cells in the spleen were most significantly elevated after R/C/N-mediated PDT combined with RT (Figure S15). Therefore, these data strongly validated that R/C/N-mediated PDT combined with RT effectively boosted systemic antitumor T-cell immunity over other monotreatment, which was the origin of efficient inhibition of cancer metastasis.

3. CONCLUSIONS

In summary, we rationally designed a biomimetic nanoplatform through a simple method for resolving the unsatisfying antitumor efficiency issue existed in separate PDT and RT. The as-constructed R/C/N nanoparticles were systematically investigated, with all the in vitro and in vivo results clearly demonstrating that R/C/N possesses superior photo-responsive efficiency, strong high-energy ionization radiation absorption ability, and excellent biocompatibility. These desirable properties allow them to realize sufficient generation of ROS, enhanced radiosensitivity, and superior systemic immune response. Taking all the results together, it becomes so encouraged that R/C/N-mediated PDT combined with RT can not only impede the growth of primary tumors but also arrest systemic metastasis to lung and liver, which was not achievable for either monotherapy. However, since the consumption of oxygen during PDT and RT can induce tumor hypoxia and limit the efficacy of these treatments, combining proper strategies to increase oxygen delivery to the tumor microenvironment during PDT and RT is a feasible approach that can further improve therapeutic outcomes.

■ ASSOCIATED CONTENT

Supporting Information

The Supporting Information is available free of charge at https://pubs.acs.org/doi/10.1021/acsami.3c03636.

Experimental details, materials, and methods; TEM image of hydrophobic UCNPs; spectral characterization of R/C/N; hydrodynamic size and zeta potential stability of UCNPs in water; UV−vis absorption spectra of DPBF under different conditions; effects of R/C/N and PDT on the DNA damage of 4T1 cells; cell apoptosis detection results; tumor section staining with chlorophosphonazo III; statistical analysis of Ki67 and TUNEL staining; weight change curve of 4T1 tumor-bearing mice after different treatments; serum biochemistry and complete blood count test results; biodistribution of R/C/N; statistical results of the number of pulmonary metastatic

https://doi.org/10.1021/acsami.3c03636
ACS Appl. Mater. Interfaces 2023, 15, 26431−26441

nodules; CRT and HMGB1 expression of tumor; H&E staining images of major organs after various treatments; and confocal fluorescence images of spleen sections after various treatments (PDF)

AUTHOR INFORMATION

Corresponding Authors

Ling Wen − *Dushu Lake Hospital Affiliated to Soochow University, Suzhou 215123, China*; Email: lingwen@suda.edu.cn

Jianfeng Zeng − *Center for Molecular Imaging and Nuclear Medicine, State Key Laboratory of Radiation Medicine and Protection, School for Radiological and Interdisciplinary Sciences (RAD-X), Collaborative Innovation Center of Radiological Medicine of Jiangsu Higher Education Institutions, Soochow University, Suzhou 215123, China*; orcid.org/0000-0001-7654-8724; Email: jfzeng@suda.edu.cn

Authors

Dandan Zhou − *Center for Molecular Imaging and Nuclear Medicine, State Key Laboratory of Radiation Medicine and Protection, School for Radiological and Interdisciplinary Sciences (RAD-X), Collaborative Innovation Center of Radiological Medicine of Jiangsu Higher Education Institutions, Soochow University, Suzhou 215123, China*; orcid.org/0000-0002-7054-4498

Yun Gao − *Center for Molecular Imaging and Nuclear Medicine, State Key Laboratory of Radiation Medicine and Protection, School for Radiological and Interdisciplinary Sciences (RAD-X), Collaborative Innovation Center of Radiological Medicine of Jiangsu Higher Education Institutions, Soochow University, Suzhou 215123, China*

Zhe Yang − *Center for Molecular Imaging and Nuclear Medicine, State Key Laboratory of Radiation Medicine and Protection, School for Radiological and Interdisciplinary Sciences (RAD-X), Collaborative Innovation Center of Radiological Medicine of Jiangsu Higher Education Institutions, Soochow University, Suzhou 215123, China*

Ning Wang − *Center for Molecular Imaging and Nuclear Medicine, State Key Laboratory of Radiation Medicine and Protection, School for Radiological and Interdisciplinary Sciences (RAD-X), Collaborative Innovation Center of Radiological Medicine of Jiangsu Higher Education Institutions, Soochow University, Suzhou 215123, China*

Jianxian Ge − *Center for Molecular Imaging and Nuclear Medicine, State Key Laboratory of Radiation Medicine and Protection, School for Radiological and Interdisciplinary Sciences (RAD-X), Collaborative Innovation Center of Radiological Medicine of Jiangsu Higher Education Institutions, Soochow University, Suzhou 215123, China*

Xiaoyi Cao − *Center for Molecular Imaging and Nuclear Medicine, State Key Laboratory of Radiation Medicine and Protection, School for Radiological and Interdisciplinary Sciences (RAD-X), Collaborative Innovation Center of Radiological Medicine of Jiangsu Higher Education Institutions, Soochow University, Suzhou 215123, China*

Dandan Kou − *Center for Molecular Imaging and Nuclear Medicine, State Key Laboratory of Radiation Medicine and Protection, School for Radiological and Interdisciplinary Sciences (RAD-X), Collaborative Innovation Center of Radiological Medicine of Jiangsu Higher Education Institutions, Soochow University, Suzhou 215123, China*

Yuan Gu − *Center for Molecular Imaging and Nuclear Medicine, State Key Laboratory of Radiation Medicine and Protection, School for Radiological and Interdisciplinary Sciences (RAD-X), Collaborative Innovation Center of Radiological Medicine of Jiangsu Higher Education Institutions, Soochow University, Suzhou 215123, China*

Cang Li − *Center for Molecular Imaging and Nuclear Medicine, State Key Laboratory of Radiation Medicine and Protection, School for Radiological and Interdisciplinary Sciences (RAD-X), Collaborative Innovation Center of Radiological Medicine of Jiangsu Higher Education Institutions, Soochow University, Suzhou 215123, China*

Mohammad Javad Afshari − *Center for Molecular Imaging and Nuclear Medicine, State Key Laboratory of Radiation Medicine and Protection, School for Radiological and Interdisciplinary Sciences (RAD-X), Collaborative Innovation Center of Radiological Medicine of Jiangsu Higher Education Institutions, Soochow University, Suzhou 215123, China*; orcid.org/0000-0001-5077-570X

Ruru Zhang − *Center for Molecular Imaging and Nuclear Medicine, State Key Laboratory of Radiation Medicine and Protection, School for Radiological and Interdisciplinary Sciences (RAD-X), Collaborative Innovation Center of Radiological Medicine of Jiangsu Higher Education Institutions, Soochow University, Suzhou 215123, China*

Can Chen − *Center for Molecular Imaging and Nuclear Medicine, State Key Laboratory of Radiation Medicine and Protection, School for Radiological and Interdisciplinary Sciences (RAD-X), Collaborative Innovation Center of Radiological Medicine of Jiangsu Higher Education Institutions, Soochow University, Suzhou 215123, China*

Shuwang Wu − *Center for Molecular Imaging and Nuclear Medicine, State Key Laboratory of Radiation Medicine and Protection, School for Radiological and Interdisciplinary Sciences (RAD-X), Collaborative Innovation Center of Radiological Medicine of Jiangsu Higher Education Institutions, Soochow University, Suzhou 215123, China*

Mingyuan Gao − *Center for Molecular Imaging and Nuclear Medicine, State Key Laboratory of Radiation Medicine and Protection, School for Radiological and Interdisciplinary Sciences (RAD-X), Collaborative Innovation Center of Radiological Medicine of Jiangsu Higher Education Institutions, Soochow University, Suzhou 215123, China*; orcid.org/0000-0002-7360-3684

Complete contact information is available at: https://pubs.acs.org/10.1021/acsami.3c03636

Notes

The authors declare no competing financial interest.

ACKNOWLEDGMENTS

The authors thank the National Key Research and Development Program of China (2018YFA0208800), the National Natural Science Foundation of China (81720108024, 82130059, 82222033, and 82172003), the Natural Science Foundation of Jiangsu Higher Education Institutions of China (20KJA150006), and the Priority Academic Program Development of Jiangsu Higher Education Institutions (PAPD) for financial support.

REFERENCES

(1) Rath, G. K.; Kumar Gandhi, A. Advances in Radiation Oncology: Current Status and Future Directions in India. *Indian J. Surg. Oncol.* **2022**, *13*, 58−60.

(2) Jacobson, G.; Galvan-Turner, V. Rethinking the Role of Radiation Therapy in the Management of Epithelial Ovarian Cancer. *Diagnostics* **2020**, *10*, 211.

(3) Hatano, K.; Tohyama, N.; Kodama, T.; Okabe, N.; Sakai, M.; Konoeda, K. Current Status of Intensity-Modulated Radiation Therapy for Prostate Cancer: History, Clinical Results and Future Directions. *Int. J. Urol.* **2019**, *26*, 775−784.

(4) Zhang, C.; Zhao, K.; Bu, W.; Ni, D.; Liu, Y.; Feng, J.; Shi, J. Marriage of Scintillator and Semiconductor for Synchronous Radiotherapy and Deep Photodynamic Therapy with Diminished Oxygen Dependence. *Angew. Chem., Int. Ed. Engl.* **2014**, *54*, 1770−1774.

(5) Barker, H. E.; Paget, J. T.; Khan, A. A.; Harrington, K. J. The Tumour Microenvironment after Radiotherapy: Mechanisms of Resistance and Recurrence. *Nat. Rev. Cancer* **2015**, *15*, 409−425.

(6) Gilreath, C.; Boerma, M.; Qin, Z.; Hudson, M. K.; Wang, S. The Hypoxic Microenvironment of Breast Cancer Cells Promotes Resistance in Radiation Therapy. *Front. Oncol.* **2021**, *10*, 629422.

(7) Fan, W.; Bu, W.; Shen, B.; He, Q.; Cui, Z.; Liu, Y.; Zheng, X.; Zhao, K.; Shi, J. Intelligent MnO2 Nanosheets Anchored with Upconversion Nanoprobes for Concurrent pH-/H2O2-Responsive UCL Imaging and Oxygen-Elevated Synergetic Therapy. *Adv. Mater.* **2015**, *27*, 4155−4161.

(8) Fan, W.; Shen, B.; Bu, W.; Zheng, X.; He, Q.; Cui, Z.; Ni, D.; Zhao, K.; Zhang, S.; Shi, J. Intranuclear Biophotonics by Smart Design of Nuclear-Targeting Photo-/Radio-Sensitizers So-Loaded Upconversion Nanoparticles. *Biomaterials* **2015**, *69*, 89−98.

(9) Liu, J.; Yang, Y.; Zhu, W.; Yi, X.; Dong, Z.; Xu, X.; Chen, M.; Yang, K.; Lu, G.; Jiang, L.; Liu, Z. Nanoscale Metal-Organic Frameworks for Combined Photodynamic & Radiation Therapy in Cancer Treatment. *Biomaterials* **2016**, *97*, 1−9.

(10) Agostinis, P.; Berg, K.; Cengel, K. A.; Foster, T. H.; Girotti, A. W.; Gollnick, S. O.; Hahn, S. M.; Hamblin, M. R.; Juzeniene, A.; Kessel, D.; Korbelik, M.; Moan, J.; Mroz, P.; Nowis, D.; Piette, J.; Wilson, B. C.; Golab, J. Photodynamic Therapy of Cancer: An Update. *Ca-Cancer J. Clin.* **2011**, *61*, 250−281.

(11) Liang, S.; Sun, C.; Yang, P.; Ma, P. A.; Huang, S.; Cheng, Z.; Yu, X.; Lin, J. Core-Shell Structured Upconversion Nanocrystal-Dendrimer Composite as a Carrier for Mitochondria Targeting and Catalase Enhanced Anti-cancer Photodynamic Therapy. *Biomaterials* **2020**, *240*, 119850.

(12) Wang, C.; Tao, H.; Cheng, L.; Liu, Z. Near-Infrared Light Induced In Vivo Photodynamic Therapy of Cancer Based on Upconversion Nanoparticles. *Biomaterials* **2011**, *32*, 6145−6154.

(13) Voon, S. H.; Kiew, L. V.; Lee, H. B.; Lim, S. H.; Noordin, M. I.; Kamkaew, A.; Burgess, K.; Chung, L. Y. In Vivo Studies of Nanostructure-Based Photosensitizers for Photodynamic Cancer Therapy. *Small* **2014**, *10*, 4993−5013.

(14) Zheng, Y. H.; Yin, G. F.; Le, V.; Zhang, A. L.; Chen, S. Y.; Liang, X.; Liu, J. W. Photodynamic-therapy Activates Immune Response by disrupting Immunity Homeostasis of Tumor Cells, which Generates Vaccine for Cancer Therapy. *Int. J. Biol. Sci.* **2016**, *12*, 120−132.

(15) Sun, X.; Cao, Z.; Mao, K.; Wu, C.; Chen, H.; Wang, J.; Wang, X.; Cong, X.; Li, Y.; Meng, X.; Yang, X.; Yang, Y. G.; Sun, T. Photodynamic Therapy Produces Enhanced Efficacy of Antitumor Immunotherapy by Simultaneously Inducing Intratumoral Rrelease of Sorafenib. *Biomaterials* **2020**, *240*, 119845.

(16) Van Limbergen, E. J.; De Ruysscher, D. K.; Olivo Pimentel, V.; Marcus, D.; Berbee, M.; Hoeben, A.; Rekers, N.; Theys, J.; Yaromina, A.; Dubois, L. J.; Lambin, P. Combining Radiotherapy with Immunotherapy: the Past, the Present and the Future. *Br. J. Radiol.* **2017**, *90*, 20170157.

(17) Garg, A. D.; Nowis, D.; Golab, J.; Agostinis, P. Photodynamic Therapy: Illuminating the Road from Cell Death towards Anti-tumour Immunity. *Apoptosis* **2010**, *15*, 1050−1071.

(18) Doix, B.; Trempolec, N.; Riant, O.; Feron, O. Low Photosensitizer Dose and Early Radiotherapy Enhance Antitumor Immune Response of Photodynamic Therapy-Based Dendritic Cell Vaccination. *Front. Oncol.* **2019**, *9*, 811.

(19) Jalani, G.; Tam, V.; Vetrone, F.; Cerruti, M. Seeing, Targeting and Delivering with Upconverting Nanoparticles. *J. Am. Chem. Soc.* **2018**, *140*, 10923−10931.

(20) Wang, M.; Chang, M.; Li, C.; Chen, Q.; Hou, Z.; Xing, B.; Lin, J. Tumor-Microenvironment-Activated Reactive Oxygen Species Amplifier for Enzymatic Cascade Cancer Starvation/Chemodynamic/Immunotherapy. *Adv. Mater.* **2022**, *34*, No. e2106010.

(21) Wang, Y.; Li, Y.; Zhang, Z.; Wang, L.; Wang, D.; Tang, B. Z. Triple-Jump Photodynamic Theranostics: MnO(2) Combined Upconversion Nanoplatforms Involving a Type-I Photosensitizer with Aggregation-Induced Emission Characteristics for Potent Cancer Treatment. *Adv. Mater.* **2021**, *33*, No. e2103748.

(22) Li, Z.; Lu, S.; Liu, W.; Dai, T.; Ke, J.; Li, X.; Li, R.; Zhang, Y.; Chen, Z.; Chen, X. Synergistic Lysozyme-Photodynamic Therapy Against Resistant Bacteria based on an Intelligent Upconversion Nanoplatform. *Angew. Chem., Int. Ed. Engl.* **2021**, *60*, 19201−19206.

(23) Zhou, J.; Liu, Q.; Feng, W.; Sun, Y.; Li, F. Upconversion Luminescent Materials: Advances and Applications. *Chem. Rev.* **2015**, *115*, 395−465.

(24) Cheng, L.; Wang, C.; Feng, L.; Yang, K.; Liu, Z. Functional Nanomaterials for Phototherapies of Cancer. *Chem. Rev.* **2014**, *114*, 10869−10939.

(25) Liu, B.; Li, C.; Yang, P.; Hou, Z.; Lin, J. 808-nm-Light-Excited Lanthanide-Doped Nanoparticles: Rational Design, Luminescence Control and Theranostic Applications. *Adv. Mater.* **2017**, *29*, 1605434.

(26) Hou, Z.; Deng, K.; Wang, M.; Liu, Y.; Chang, M.; Huang, S.; Li, C.; Wei, Y.; Cheng, Z.; Han, G.; Al Kheraif, A. A.; Lin, J. Hydrogenated Titanium Oxide Decorated Upconversion Nanoparticles: Facile Laser Modified Synthesis and 808 nm Near-Infrared Light Triggered Phototherapy. *Chem. Mater.* **2019**, *31*, 774−784.

(27) Chen, X.; Song, L.; Li, X.; Zhang, L.; Li, L.; Zhang, X.; Wang, C. Co-delivery of Hydrophilic/Hydrophobic Drugs by Multifunctional Yolk-shell Nanoparticles for Hepatocellular Carcinoma Theranostics. *Chem. Eng. J.* **2020**, *389*, 124416.

(28) Wei, Z.; Duan, G.; Huang, B.; Qiu, S.; Zhou, D.; Zeng, J.; Cui, J.; Hu, C.; Wang, X.; Wen, L.; Gao, M. Rational Designed Rapid Liver Clearance Rare-earth Core-shell Nanoprobe for Dual-Modal Breast Cancer Imaging in the Second Near-Infrared Window. *J. Nanobiotechnol.* **2021**, *19*, 369−383.

(29) Zhao, M.; Li, B.; Wang, P.; Lu, L.; Zhang, Z.; Liu, L.; Wang, S.; Li, D.; Wang, R.; Zhang, F. Supramolecularly Engineered NIR-II and Upconversion Nanoparticles In Vivo Assembly and Disassembly to Improve Bioimaging. *Adv. Mater.* **2018**, *30*, 1804982.

(30) Shen, J.; Chen, G.; Ohulchanskyy, T. Y.; Kesseli, S. J.; Buchholz, S.; Li, Z.; Prasad, P. N.; Han, G. Upconversion: Tunable Near Infrared to Ultraviolet Upconversion Luminescence Enhancement in (α-NaYF4:Yb,Tm)/CaF2 Core/Shell Nanoparticles for In situ Real-time Recorded Biocompatible Photoactivation (Small 19/2013). *Small* **2013**, *9*, 3212.

(31) Xie, J.; Gong, L.; Zhu, S.; Yong, Y.; Gu, Z.; Zhao, Y. Emerging Strategies of Nanomaterial-Mediated Tumor Radiosensitization. *Adv. Mater.* **2018**, *31*, 1802244.

(32) Ding, B.; Zheng, P.; Jiang, F.; Zhao, Y.; Wang, M.; Chang, M.; Ma, P.; Lin, J. MnO(x) Nanospikes as Nanoadjuvants and Immunogenic Cell Death Drugs with Enhanced Antitumor Immunity and Antimetastatic Effect. *Angew. Chem., Int. Ed. Engl.* **2020**, *59*, 16381−16384.

(33) Gao, W.; Hu, C. M.; Fang, R. H.; Luk, B. T.; Su, J.; Zhang, L. Surface Functionalization of Gold Nanoparticles with Red Blood Cell Membranes. *Adv. Mater.* **2013**, *25*, 3549−3553.

(34) Zhang, Q.; Zhou, D.; Fang, G.; Lu, H.; Zeng, J.; Gu, Z. Cell-Derived Biomimetic 2D Nanoparticles to Improve Cell Specific Targeting and Tissue Penetration for Enhanced Magnetic Resonance Imaging. *Adv. Mater. Interfac.* **2022**, *9*, 2101914.

https://doi.org/10.1021/acsami.3c03636
ACS Appl. Mater. Interfaces 2023, 15, 26431−26441

(35) Li, M.; Fang, H.; Liu, Q.; Gai, Y.; Yuan, L.; Wang, S.; Li, H.; Hou, Y.; Gao, M.; Lan, X. Red Blood Cell Membrane-coated Upconversion Nanoparticles for Pretargeted Multimodality Imaging of Triple-negative Breast Cancer. *Biomater. Sci.* **2020**, *8*, 1802−1814.
(36) Ben-Akiva, E.; Yu, H.; Smith, J. T.; DrewPardoll, M.; Jordan, J. Biomimetic Anisotropic Polymeric Nanoparticles Coated with Red Blood Cell Membranes for Enhanced Circulation and Toxin Removal. *Sci. Adv.* **2020**, *6*, No. eaay9035.
(37) Fang, H.; Li, M.; Liu, Q.; Gai, Y.; Yuan, L.; Wang, S.; Zhang, X.; Ye, M.; Zhang, Y.; Gao, M.; Hou, Y.; Lan, X. Ultra-sensitive Nanoprobe Modified with Tumor Cell Membrane for UCL/MRI/PET Multi-modality Precise Imaging of Triple-Negative Breast Cancer. *Nano-Micro Lett.* **2020**, *12*, 62−76.
(38) Gao, M.; Hu, A.; Sun, X.; Wang, C.; Dong, Z.; Feng, L.; Liu, Z. Photosensitizer Decorated Red Blood Cells as an Ultrasensitive Light-Responsive Drug Delivery System. *ACS Appl. Mater. Interfaces* **2017**, *9*, 5855−5863.
(39) Chauhan, V. P.; Popovic, Z.; Chen, O.; Cui, J.; Fukumura, D.; Bawendi, M. G.; Jain, R. K. Fluorescent Nanorods and Nanospheres for Real-time In Vivo Probing of Nanoparticle Shape-dependent Tumor Penetration. *Angew. Chem., Int. Ed. Engl.* **2011**, *50*, 11417−11420.
(40) Zhao, Y.; Wang, Y.; Ran, F.; Cui, Y.; Liu, C.; Zhao, Q.; Gao, Y.; Wang, D.; Wang, S. A Comparison Between Sphere and Rod Nanoparticles Regarding Their In Vivo Biological Behavior and Pharmacokinetics. *Sci. Rep.* **2017**, *7*, 4131.
(41) Hochmuth, R. M.; Evans, C. A.; Wiles, H. C.; McCown, J. T. Mechanical Measurement of Red Cell Membrane Thickness. *Science* **1983**, *220*, 101−102.
(42) Huang, J.; Hou, Y.; Ma, T.; Zhang, P.; Li, Y.; Liu, C.; Zhang, B.; Qiu, S.; Zeng, J.; Gao, M. A Novel Histochemical Staining Approach for Rare-Earth-Based Nanoprobes. *Adv. Ther.* **2018**, *1*, 1800005.
(43) Burnette, B.; Weichselbaum, R. R. Radiation as an Immune Modulator. *Semin. Radiat. Oncol.* **2013**, *23*, 273−280.
(44) Zhang, P.; Miska, J.; Lee-Chang, C.; Rashidi, A.; Panek, W. K.; An, S.; Zannikou, M.; Lopez-Rosas, A.; Han, Y.; Xiao, T.; Pituch, K. C.; Kanojia, D.; Balyasnikova, I. V.; Lesniak, M. S. Therapeutic Targeting of Tumor-associated Myeloid Cells Synergizes with Radiation Therapy for Glioblastoma. *Proc. Natl. Acad. Sci. U.S.A.* **2019**, *116*, 23714−23723.
(45) Guan, X.; Sun, L.; Shen, Y.; Jin, F.; Bo, X.; Zhu, C.; Han, X.; Li, X.; Chen, Y.; Xu, H.; Yue, W. Nanoparticle-enhanced Radiotherapy Synergizes with PD-L1 Blockade to Limit Post-surgical Cancer Recurrence and Metastasis. *Nat. Commun.* **2022**, *13*, 2834.
(46) Chen, Q.; Xu, L. G.; Liang, C.; Wang, C.; Peng, R.; Liu, Z. Photothermal Therapy with Immune-adjuvant Nanoparticles Together with Checkpoint Blockade for Effective Cancer Immunotherapy. *Nat. Commun.* **2016**, *7*, 13193.
(47) Jiang, Y.; Huang, J.; Xu, C.; Pu, K. Activatable Polymer Nanoagonist for Second Near-infrared Photothermal Immunotherapy of Cancer. *Nat. Commun.* **2021**, *12*, 742.

https://doi.org/10.1021/acsami.3c03636
ACS Appl. Mater. Interfaces 2023, 15, 26431−26441